Research Paper

Modelling the effect of round window stiffness on residual hearing after cochlear implantation

CrossMark

Stephen J. Elliott [a], Guangjian Ni [a, c, *], Carl A. Verschuur [a, b]

[a] Institute of Sound and Vibration Research, University of Southampton, Southampton, SO17 1BJ, UK
[b] University of Southampton Auditory Implant Service, Southampton, SO17 1BJ, UK
[c] Laboratory of Modern Acoustics of MOE, Nanjing University, Nanjing, 210093, China

ABSTRACT

Preservation of residual hearing after cochlear implantation is now considered an important goal of surgery. However, studies indicate an average post-operative hearing loss of around 20 dB at low frequencies. One factor which may contribute to post-operative hearing loss, but which has received little attention in the literature to date, is the increased stiffness of the round window, due to the physical presence of the cochlear implant, and to its subsequent thickening or to bone growth around it. A finite element model was used to estimate that there is approximately a 100-fold increase in the round window stiffness due to a cochlear implant passing through it. A lumped element model was then developed to study the effects of this change in stiffness on the acoustic response of the cochlea. As the round window stiffness increases, the effects of the cochlear and vestibular aqueducts become more important. An increase of round window stiffness by a factor of 10 is predicted to have little effect on residual hearing, but increasing this stiffness by a factor of 100 reduces the acoustic sensitivity of the cochlea by about 20 dB, below 1 kHz, in reasonable agreement with the observed loss in residual hearing after implantation. It is also shown that the effect of this stiffening could be reduced by incorporating a small gas bubble within the cochlear implant.

© 2016 The Authors. Published by Elsevier B.V. This is an open access article under the CC BY license (http://creativecommons.org/licenses/by/4.0/).

1. 1introduction

There is increasing interest in the preservation of residual low-frequency hearing after cochlear implantation. This is partially motivated by the observation that residual low-frequency hearing can be used in a complimentary way to electrical excitation from the cochlear implant to give significantly improved speech perception (Causon et al., 2015; Helbig et al., 2011). This improvement is thought to be partially due to better pitch perception (Talbot and Hartley, 2008) and better recognition of the fundamental frequency and first formant (Verschuur et al., 2013; Zhang et al., 2010). Improved timing cues are also important (Gifford et al., 2013), because these cues are more effectively coded by the auditory system and are highly degraded by current cochlear

implant signal processing and the spread of electrical excitation associated with cochlear implant stimulation. There may be additional benefits to cochlear structure preservation because of potential future therapies, such as hair cell regeneration (Rubel et al., 2013), and because better cochlear health has been shown to be related to better electrical hearing (Pfingst et al., 2015).

Published studies of hearing preservation after cochlear implantation have typically shown post-operative hearing loss around 20–25 dB. As an example, Fig. 1 shows the calculated average loss in residual hearing, measured within six months of surgery in 104 implanted ears by Verschuur et al. (2016). The average loss of residual hearing after cochlear implantation is seen to be about 22 dB at 100 Hz, falling to about 12 dB at 1 kHz. These changes in residual hearing are in reasonable agreement with measurements of average changes in threshold values made at other cochlear implant (CI) centres (Adunka et al., 2013; Friedmann et al., 2015) and also shown in two recent meta-analyses of published hearing preservation data (Causon et al., 2015; Santa Maria et al., 2014). The variance of the residual hearing loss between patients in Verschuur et al. (2016) is quite large, which is also typical of published studies of hearing preservation after cochlear implantation. A range of

---
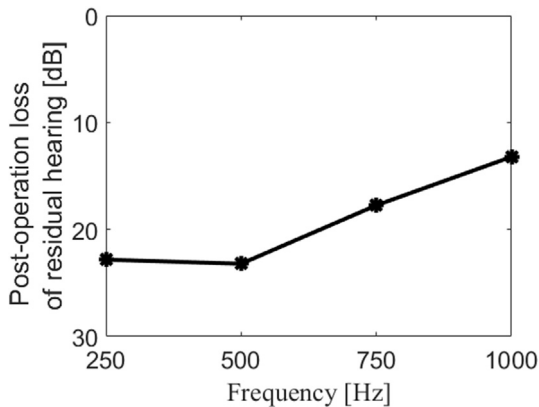
Fig. 1. The mean values of hearing loss due to cochlear implantation, calculated from the mean of the differences between pre-operative and post-operative pure-tone audiometric thresholds, for cochlear implant recipients at the University of Southampton Auditory Implant Service (Verschuur et al., 2016).

factors have been shown to underpin post-operative hearing loss, including chronic inflammation and the development of fibrotic tissue within the cochlea, which may be particularly implicated in longer-term loss of residual hearing (Causon et al., 2015). However, one possible mechanism for the loss of residual hearing that has received little attention in the literature is the stiffening of the round window (RW), either because of the presence of the cochlear implant itself, or due to the subsequent growth of bone or fibrotic tissue around it. This is particularly relevant given the wide-spread use of the direct round window approach in hearing preservation surgery (Richard et al., 2012).

Deliberate round window occlusion has been used as a method to reduce symptoms associated with superior semicircular canal dehiscence (Nikkar-Esfahani et al., 2013; Silverstein et al., 2014) with the majority of patients reporting no change in hearing loss. However, in superior semicircular canal dehiscence the "third window" effect which is characteristic of the condition may prevent round window occlusion leading to further hearing loss, whereas a link between round window occlusion and both sensorineural and conductive hearing loss has been shown in both animal and human studies. Round window occlusion has been shown to be implicated in hearing loss associated with otosclerosis (Grant, 1973). Nageris et al. (2012) showed a 30 dB conductive hearing loss due to fixation of the round window with glue in a group of rats. Cai et al. (2013) also showed a reduction in auditory brainstem response thresholds and in the slope of distortion product otoacoustic emission input-output functions in rats as a result of round window fixation with adhesive. Quesnel et al. (2016) reported a histopathological study of an individual who showed loss of residual hearing after cochlear implantation with evidence of bone growth and fibrotic changes in the basal turn of the cochlea and concomitant reduction in round window compliance. Crucially, there was an absence of measurable changes in hair cell or spiral ganglion cell populations, suggestive of a mechanism of post-operative hearing loss due to changes to cochlear mechanics rather than in neurosensory transduction. Although this is a histopathological finding from one individual, it has wider ramifications for cochlear implant users given that fibrotic changes in the cochlea consequent to cochlear implantation are likely to be wide-spread (e.g. Seyyedi and Nadol, 2014).

In this paper the effect on acoustic hearing of increasing the round window stiffness is predicted, in order to help understand the role that this mechanism may play in the loss of residual hearing after cochlear implantation.

A finite element model of the round window is first developed in order to estimate the increase in its stiffness due to the presence of a cochlear implant passing through it. A lumped element model is then used to predict the effect of this stiffening on the residual hearing. The development of this lumped element model is discussed, together with the estimation of its parameters. The cochlear input impedance and the acoustic impedance at the tympanic membrane are then calculated using the model and are shown to be similar to that previously measured if the normal value for the stiffness of the round window is assumed, but are seen to get significant larger at some frequencies if the round window stiffness is increased. The lumped element model is then used to predict the reduction in pressure difference across the basilar membrane, and hence the hearing loss, due to an increase in round window stiffness. The variability of this predicted loss in residual hearing is also calculated when using reasonable variations in the values of the assumed physical parameters, and a potential method for the mitigation of the effects of a stiffening window is finally described.

2. Finite element model of the round window

A finite element model of the round window is developed here to investigate the effect of stiffening due to a cochlear implant. The round window is initially modelled as a thin, circular flat plate (Kwacz et al., 2013) and is assumed to have a diameter of 2 mm, and a thickness of 70 μm (Zhang and Gan, 2013). The edge of the round window is assumed to be clamped (Li et al., 2007; Toth et al., 2006). Although the round window is known to have a saddle-shaped curvature and its shape is not quite round, and is also known to be subject to significant individual differences, Li et al. (2007), Atturo et al. (2014), these effects will mainly influence its high frequency dynamics, rather than the low frequency stiffness of interest here. The Young's modulus is assumed to be 1×10^6 Pa and the density of the round window to be 1200 kg m^{-3}, in order to produce a similar frequency response to that obtained for the vibration of the round window in air by Zhang and Gan (2013). This model has been extended, using Ansys (v15.0), to include a fluid on one side. The membrane is meshed with 864 "solid185" elements, which model 3D elastic structures, and the fluid as 5184 "fluid30" elements, which includes the 3D inertia and compliance of the fluid, where the combination of these two elements is a common choice for modelling fluid-structure interaction. Fig. 2 shows the resulting deflection and near-field pressure distributions, when driven by a uniform driving pressure at a frequency of 0.1 kHz. The stiffening effect due to insertion of a cochlear implant is then simulated by assuming that the round window is also clamped around a circular central disc, having a diameter of 1 mm. The acoustic input impedance of the round window is calculated from the ratio of driving pressure to the round window volume velocity, which is the accumulation of the predicted nodal velocities multiplied by their elemental area, and is plotted as a function of frequency in Fig. 3, both when intact and when clamped at the central disc.

This model clearly simplifies the actual condition of the round window with a cochlear implant inserted through it in a number of respects. First, the cochlear implant is assumed to pass centrally through the round window, although other finite element simulations, not shown here, indicate that the change in response is relatively small if the insertion is off-centre. Second, it is assumed that the cochlea implant is immobile, i.e. the inner disc does not move, although there may be some residual movement of the cochlear implant in practice (Semmelbauer and Böhnke, 2016). Finally, and probably most importantly, it is assumed that the distribution of the thickness and material properties of the round window are uniform and unaffected by the insertion of the cochlea
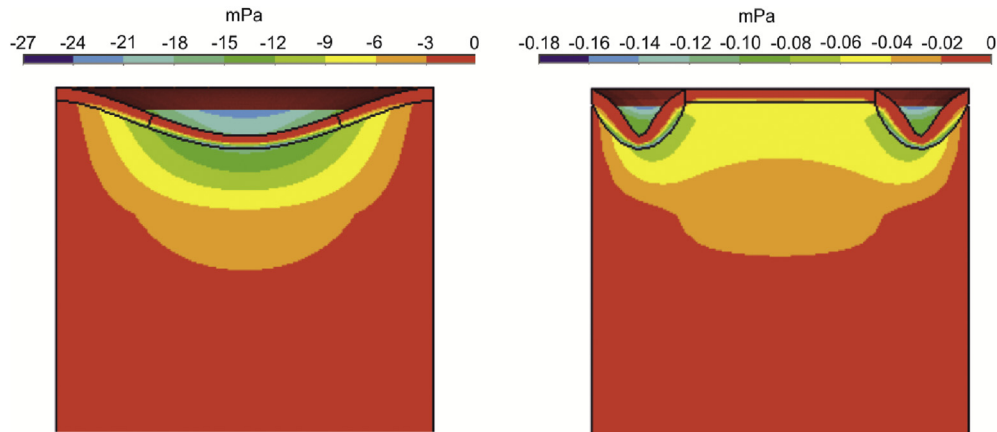
Fig. 2. Results of the finite element model for the deflection of the round window with fluid on one side and pressure contours in the fluid when it is driven inward by a uniform pressure of 1 Pa at a frequency of 0.1 kHz. Intact round window (left), and round window with cochlear implant which is assumed to be fixed (right).
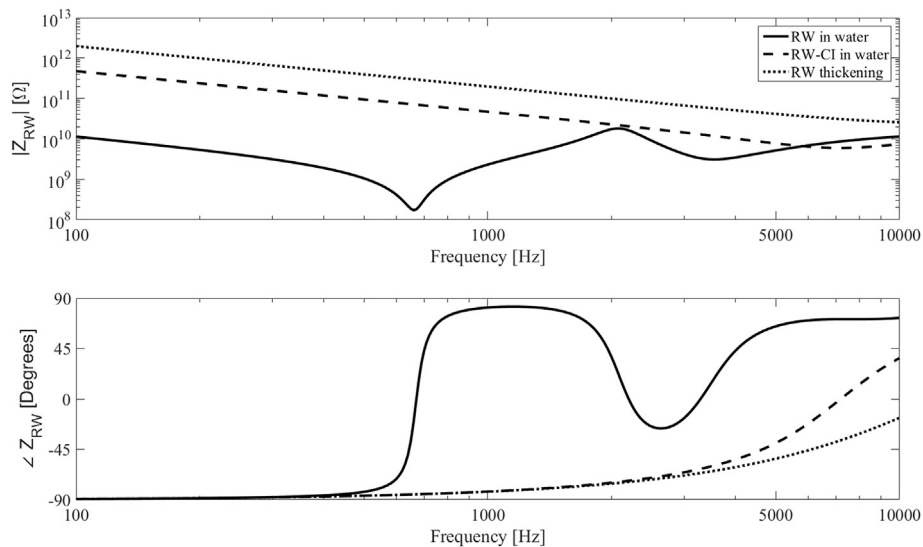
Fig. 3. The magnitude and phase of the round window acoustic impedance calculated at three conditions: namely intact round window (RW in water), with a cochlear implant inserted and fixed through the round window (RW-CI in water), and with the cochlear implant and a doubling of round window thickness (RW thickening).

implant and the subsequent healing around it, whereas there is likely to be a thickening of the round window close to the cochlear implant. Overall, however, the model shown in Fig. 2 provides a convenient first approximation to calculate the stiffening effect of the cochlea implant on the round window dynamics.

The acoustic impedance predicted for the intact round window up to about 2 kHz is similar to that measured by Nakajima et al. (2009), as discussed in Appendix A. It has a low frequency acoustic compliance of about $1.4 \times 10^{-13} \, N^{-1} \, m^5$ and an impedance null, indicating a mechanical resonance, at a frequency of about 650 Hz, suggesting that the effective mass is about 4 mg if this response is modelled as a single degree of freedom system. There is also an additional dip in the modulus of the impedance, at about 3.5 kHz, which appears as a higher order radial mode of the round window in the finite element results. The calculated mass of the round window itself is only about 0.2 mg and so the bulk of the effective mass is due to the entrained fluid. The motion of the RW is almost in phase at each node for driving frequencies below about 1 kHz, in agreement with the measurements of Stenfelt et al. (2004) and Kwacz et al. (2011). In this flat, uniform and symmetric model, the asymmetrical modes of the RW observed at higher frequencies by

these authors are not excited, although these only occurred outside the frequency range of interest here. When the round window is clamped around a disc at its centre, but its thickness is unaltered, the low-frequency stiffness is increased by a factor of about 40. The frequency of the first null in the impedance curve is then increased to about 7.2 kHz, indicating a reduction in the effective mass to about 0.8 mg, due to the reduction in volume of the entrained fluid. Also shown in Fig. 3 is the acoustic impedance calculated from the finite element model of the round window and immobile disc, when the thickness of the round window is increased, from 70 μm to 140 μm. The low-frequency stiffness is increased by a factor of about 170 in this case. If the diameter of the cochlear implants is assumed to be 0.5 mm rather than 1 mm, the stiffness increases by a about a factor of 10, or about a factor of 40 if the thickness of the round window is again assumed to be double. Talking into account the uncertainty in the likely thickening of the round window after implantation, an increase in stiffness by a factor of 100 appears to be reasonable order-of-magnitude assumption.
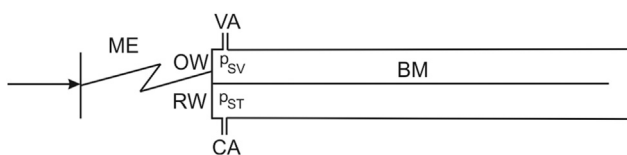
It is only the general form of the round window impedance, up to about 1 kHz, which is used in the lumped element model below, and so the accuracy of the detailed response above this frequency

will not affect the subsequent results in this paper. This more detailed response is likely to be affected by the fact that the round window is not completely flat (Atturo et al., 2014; Li et al., 2007), the anisotropy of its structure, giving rise to asymmetrical motion (Kwacz et al., 2011; Stenfelt et al., 2004), and the variability between subjects (Kwacz et al., 2011). Another factor that may lead to a stiffening of the round window after implantation is bone growth in this area. Quesnel et al. (2016) discuss an interesting case study in which bone growth was observed in histopathology for a patient who had a cochlear implant via cochleostomy seven years prior to death. These authors also discuss the increased impedance of the round window as a possible cause of loss in residual hearing. Although this particular patient experienced severe loss of residual hearing between 4 and 8 weeks after surgery and was found at post-mortem to have bone growth over the whole of the round window, such bone growth may occur in other patients over just a part of the round window and hence contribute to its stiffening. Quesnel et al. (2016) also observed growth in loose fibrotic tissue in the scala tympani close to the round window. The effect of this fibrotic tissue has been studied by Choi and Oghalai (2005) by increasing the fluid damping in a transmission line model and they predicted a significant effect on the basilar membrane velocity if this damping was increased by a factor of 1000.

3. Lumped element model

The aim of this paper is to predict the change in residual hearing due to increases in the stiffness of the round window. It is assumed that the mechanism of slow wave propagation along the cochlea is unaffected by this change in round window stiffness, but that it is the excitation of this wave, by the pressure difference across the basilar membrane at the base of the cochlea, that is altered. It is well known that the ratio of this pressure difference to the alternating volume velocity in each of the fluid chambers is almost real and independent of frequency (Zwislocki, 1962; Puria and Allen, 1991), and this may be termed the acoustic wave impedance, Z_{WA}. Physically, the wave impedance is determined by the properties of the forward travelling wave at the base of the cochlea since, under normal hearing conditions, any reflected wave has a much lower amplitude, and so it is analogous to the, real, characteristic impedance in a waveguide or transmission line.

A simplified sketch of the middle ear and the uncoiled cochlea is shown in Fig. 4. As well as the oval window (OW) and round window (RW) this also includes the vestibular aqueduct (VA) in the scala vestibuli (SV) and the cochlear aqueduct (CA) in the scala tympani (ST). This representation of the fluid pathways is clearly a simplification, since the VA actually connects to the vestibule rather than the cochlear fluid chamber for example, but it does provide a reasonable representation for our purposes. An idealisation of the middle ear (ME), as driven by the eardrum, is also shown in Fig. 4. The acoustic pressure at the base of the scala vestibuli, p_{SV}, is driven
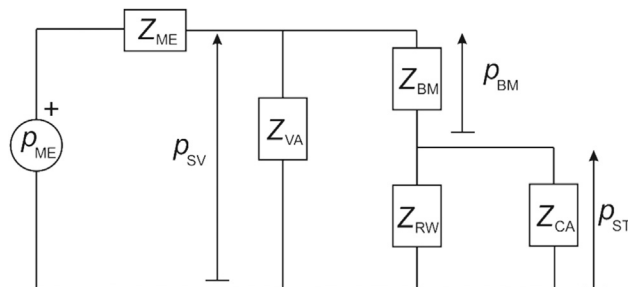
by the pressure at the eardrum by the dynamics of the middle ear. The pressure at the base of the scala tympani, p_{ST}, is determined by the volume velocity in this chamber and the terminating impedance at the round window. Since there is no wave propagation involved in the dynamic behaviour in both of these places, it is reasonably well approximated by a lumped element model, as described in this section. The historical development of lumped element models of the cochlea has recently been discussed by Marquardt and Hensel (2013) who described the earlier models of Dallos (1970), Lynch et al. (1982) and Franke et al. (1985). Stenfelt (2015) has also recently used a lumped element model to estimate the different contributions to bone conduction.

Fig. 5 shows the lumped element model of this system used in the present study. The middle ear is represented by its Thévenin equivalent blocked pressure response, p_{ME}, and its internal impedance, Z_{ME}, which is the impedance seen by the pressure in the SV looking out into the middle ear, and includes the dynamics of the oval window. The pressure in the SV is the sum of the pressure difference across the BM, p_{BM}, and the pressure in the ST, p_{ST}.

It should be emphasised that p_{SV} and p_{ST} are assumed to be measured some distance away from the vibrating windows, and so any near-field components of the pressure in these chambers are excluded from p_{SV} and p_{ST}. These near-field pressures do, however, give rise to inertances, which are accounted for in Z_{ME} and Z_{RW}. The impedance Z_{BM} relates the pressure across the BM, p_{BM}, to the volume velocity entering the fluid chambers and is largely resistive. Under normal circumstances p_{ST} would be much smaller than p_{BM}, since the impedance of the round window, Z_{RW}, would be much smaller than Z_{BM}. As the stiffness of the round window increases, however, this is no longer true and Z_{RW} can become so large that the impedances of the cochlear and vestibular aqueducts, Z_{CA} and Z_{VA}, which are normally too large to play a significant part in the generation of p_{BM}, also become important. The form of these individual impedances is described in the following section.

The basilar membrane response all the way along the cochlea, at any given frequency, will be entirely determined by the pressure difference driving the basilar membrane at the base, so that the peak in the response of the cochlea at the characteristic place, for example, is originally excited by the pressure difference at the base. The hearing response will thus be directly proportional to the pressure p_{BM} in Fig. 5 and no explicit model of wave propagation along the cochlea is required, which is a powerful feature of such lumped element models. This will be true whether the cochlea is entirely passive or whether it retains any element of the cochlear amplifier. The change in the pressure difference at the base of the cochlea can be investigated by considering the change in the acoustic pressure at the base of each of the fluid chambers.

Fig. 4. A diagrammatic representation of the middle ear and the uncoiled cochlea to show the arrangement at its base. The middle ear, ME, drives the scala vestibuli, SV, via the stapes and oval window, OW, to give the pressure, p_{SV}, which excites the pressure difference across the basilar membrane, p_{BM}, which is equal to $p_{SV} - p_{ST}$, where p_{ST} is the pressure in the scala tympani, ST, opposite the round window, RW. The vestibular aqueduct, VA, and cochlear aqueduct, CA, are also found to be important when the round window becomes stiffer.

Fig. 5. The impedance model used to study the effect of round window stiffness, included in Z_{RW}, on the pressure across the basilar membrane, p_{BM}, which is the difference between the pressure in the scala vestibuli, p_{SV} and that in the scala tympani p_{ST}, where p_{ME} and Z_{ME} are the Thévenin equivalent source and impedance of the middle ear, Z_{BM} is the impedance across the basilar membrane and Z_{VA} and Z_{CA} are the impedances of the vestibular and cochlear aqueducts.

4. Estimation of the individual impedances

4.1. Middle ear impedance

A Thévenin equivalent circuit (Van Valkenburg, 1974) is used for the middle ear, so Z_{ME} is the impedance looking out of the cochlea into the middle ear, with no external excitation. The impedance Z_{ME} is thus the same as the parameter M3 in the analysis of Puria (2003), who fits a lumped element, mass-spring-damper, model to this impedance so that it is modelled as

$$Z_{ME} = i\omega L_{ME} + R_{ME} + \frac{1}{i\omega C_{ME}}, \tag{1}$$

where Z_{ME} is the ratio of pressure to volume velocity, so that C_{ME}, R_{ME} and L_{ME} are the acoustic compliance, resistance and inertance of the middle ear. This is shown explicitly in Fig. 6, together with the final form of the other impedances indicated in Fig. 5. The values of these parameters estimated for the human ear by Puria (2003) are listed in Table 1, together with the values of all of the other parameters used in this model. The combination of p_{ME} and Z_{ME} in this Thévenin equivalent circuit provides a complete description of the behaviour of the middle ear as seen by the oval window. The physical interpretation of the pressure p_{ME} is that it is the pressure that would be exerted on the stapes, if the stapes were entirely blocked. This pressure is directly proportional to the pressure in the ear canal, because of linearity, and is unaffected by any changes in the round window stiffness. The Thévenin equivalent circuit thus provides a convenient description of the middle ear for our purposes, with a single internal impedance, Z_{ME}, and a source term, p_{ME}, that is directly proportional to the excitation in the ear canal.

4.2. Impedance across the basilar membrane

The ratio of the pressure across the basilar membrane to the volume velocity that travels down the scala at the base of the cochlea is denoted Z_{BM} and this is made up of two components. The first is a result of the propagation of the slow wave down the cochlea, and is largely resistive, so will be denoted R_{WA}, and is estimated to be 2×10^{10} N s m^{-5} by Aibara et al. (2001), for example.

The other component is due to the inertance of the fluid in the two chambers, L_{FL}. These two impedances appear in parallel, since they are driven by the same pressure difference. The acoustic inertance, L, of the fluid in a tube of length l and area A is given by

$$L = \frac{\rho l}{A}. \tag{2}$$

This expression can be used to estimate L_{FL} for the two fluid chambers in the cochlea assuming that l is equal to twice the length of the human cochlea, i.e. 70 mm, and that its area is 1 mm^2, to give a value of L_{FL} of about 7.0×10^7 N s^2 m^{-5}, in reasonable agreement with Marquardt and Hensel (2013).

The magnitude of the impedance, ωL_{FL}, due to the fluid inertia, is greater than that of the assumed wave impedance above about 20 Hz, and so the presence of this inertance does not significantly affect Z_{BM} in the frequency range of interest here, which is above 100 Hz, but is included for completeness. In fact the fluid impedance is also increased by the impedance of the helicotrema, as discussed by Dallos (1970) and Lynch et al. (1982), but this is ignored here, since it would only act to the lower frequency above which R_{WA} is dominant in the parallel combination of R_{WA} and L_{FL}.

4.3. Round window

The acoustic impedance of the round window, together with the associated entrained fluid, has been measured by Nakajima et al. (2009). In Appendix A, a minor correction is applied to these measurements in order to account for the rocking of the stapes, since the volume velocity in the experiments was estimated from the linear velocity at the edge of the stapes. With this correction, the acoustic impedance of the round window under normal conditions is found to be reasonably well approximated, up to about 5 kHz, by a mass-spring-damper model such that

$$Z_{RW} = i\omega L_{RW} + R_{RW} + \frac{1}{i\omega C_{RW}}, \tag{3}$$

where the values of the acoustic compliance, resistance and inertance deduced from Appendix A are listed in Table 1. The value of the RW compliance under these normal conditions is denoted C_{RW}^0
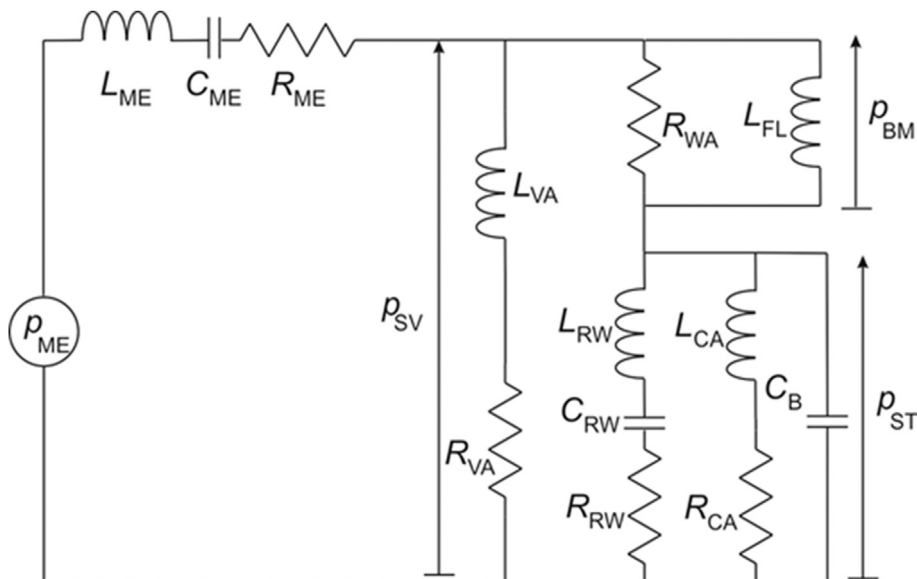

Fig. 6. The complete equivalent circuit diagram of the lumped element model used to analyse the effect of changing the round window stiffness, $1/C_{RW}$, on the pressure across the BM, p_{BM}.

Table 1
Parameter values used in the lumped element model and their source.

Name	Parameter	SI units	Value	Source
Middle ear inertance	L_{ME}	N s^2 m^{-5}	4.4×10^5	(Puria, 2003)
Middle ear compliance	C_{ME}	N^{-1} m^5	1.2×10^{-14}	
Middle ear resistance	R_{ME}	N s m^{-5}	1.0×10^{10}	
Wave impedance	R_{WA}	N s m^{-5}	2.0×10^{10}	(Aibara et al., 2001)
RW inertance	L_{RW}	N s^2 m^{-5}	1.0×10^6	Fitted based on
RW resistance	R_{RW}	N s m^{-5}	2.5×10^9	(Nakajima et al., 2009)
Nominal RW compliance	C_{RW}^0	N^{-1} m^5	1.0×10^{-13}	
Vestibular aqueduct inertance	L_{VA}	N s^2 m^{-5}	5.1×10^7	
Cochlear aqueduct inertance	L_{CA}	N s^2 m^{-5}	5.6×10^8	Appendix B, based on (Stenfelt, 2015)
Vestibular aqueduct resistance	R_{VA}	N s m^{-5}	$1.1 \times 10^{10} \times \sqrt{f/1 \text{ kHz}}$	
Cochlear aqueduct resistance	R_{CA}	N s m^{-5}	$3.5 \times 10^{11} \times \sqrt{f/1 \text{ kHz}}$	

in Table 1, since this will be divided by various factors to provide the increase in round window stiffness used in the later simulations. This assumed compliance is also in good agreement with the prediction of the finite element model in Section 2.

4.4. Impedance of the aqueducts

The elements Z_{VA} and Z_{CA} in Fig. 5 represent the acoustic impedances of the vestibular aqueduct and the cochlear aqueduct. Stenfelt (2015) has modelled these impedances as comprising the inertance and resistance of the aqueducts together with the compliance of a cranial space. The form of this acoustic impedance is discussed in Appendix B, where it is shown that over the frequency range of interest here, it is well approximated by only its inertance and resistance, although this resistance is weakly frequency-dependent.

The values of the acoustic inertances and resistances have been calculated using the equations in Appendix B, with the lengths and areas of the two aqueducts, as suggested by Stenfelt (2015), who assumed that the length of the cochlear aqueduct was 10 mm and that it diameter was 0.15 mm, and that the vestibular aqueduct was made up of a tube of length 1.5 mm with a diameter of 0.3 mm, in series with a tube of length 8.5 mm and a diameter of 0.6 mm. The assumed values of these inertance and resistance values are given in Table 1, although it should be noted that these are probably the least reliable parameters in the lumped element model. Significant individual differences in the sizes of the aqueducts and their patency have been noted by Gopen et al. (1997) and Saliba et al. (2012), as discussed further in Section 7. This variability is less important under normal hearing conditions, since the impedance of the aqueducts is then always large compared to the impedance of the round window, but it becomes more important as the round window is stiffened and the impedance of the aqueducts has a larger effect. Other fluid connections from the cochlea, such as the leaks due to vessels or nerves, will also affect the response to some extent, but these can be assumed to be lumped in with the impedances of the aqueducts in Fig. 5.

The overall circuit diagram for these components is shown in Fig. 6, together with an additional impedance, C_B, to be discussed in Section 8. The magnitudes of the impedances for these individual components are shown on a log-log scale in Fig. 7 to illustrate their relative values at different frequencies, following Marquardt and Hensel (2013), as will be used below.

5. prediction of input impedance at the stapes and the tympanic membrane

Although the main objective of this paper is to predict the effect of increases in the round window stiffness on hearing levels, the lumped element model presented above also readily allows the prediction of the changes in cochlear input impedance as the round window stiffness increases. This can then be used to predict the consequent changes in the impedance at the tympanic membrane. These results are included here since they may provide an easier method of experimentally validating the lumped element model than using the rather more inaccessible changes in the pressure across the BM.

The cochlear input impedance, Z_C, which is the ratio of the pressure in the SV to the stapes volume velocity can be derived from Fig. 5 as

$$Z_C = \frac{Z_{VA}(Z_{BM}Z_{RW} + Z_{BM}Z_{CA} + Z_{CA}Z_{RW})}{(Z_{VA} + Z_{BM})(Z_{RW} + Z_{CA}) + Z_{CA}Z_{RW}}. \tag{4}$$
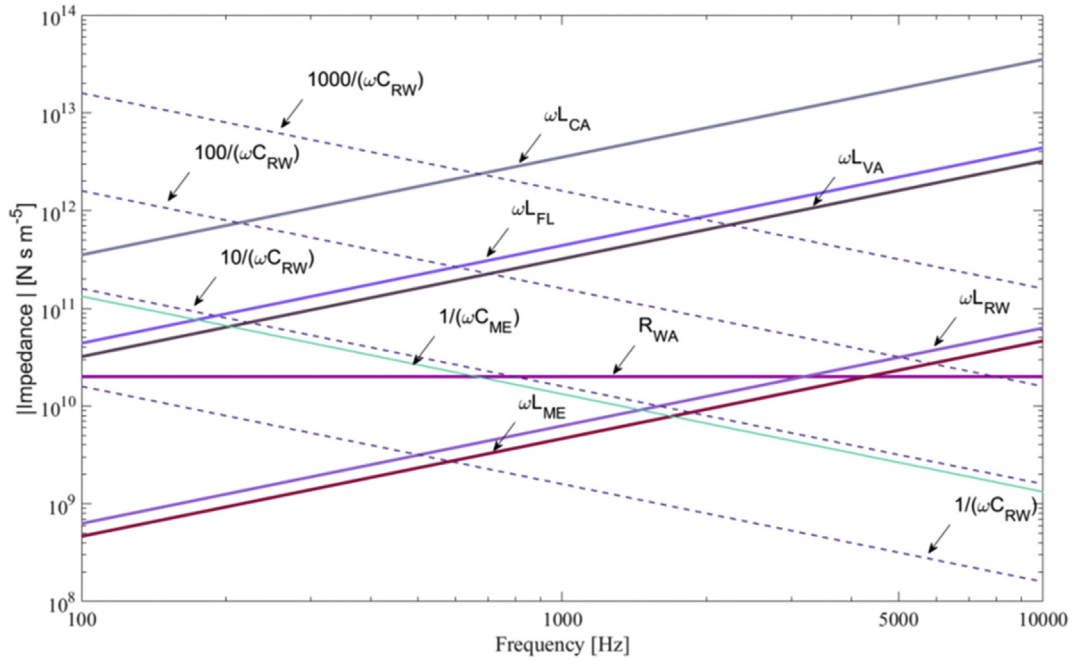
Fig. 8 shows the calculated magnitude and phase of Z_C when the compliance of the round window takes its normal value and when it is decreased by a factor of 10, 100 or 1000. Under normal conditions Z_{RW} is significantly less than R_{WA} up to about 3 kHz, and so Z_C is mainly resistive at low frequencies, as measured by Aibara et al. (2001), Puria (2003) and Nakajima et al. (2009) for example. Above about 5 kHz the inertance associated with the round window is predicted to become more important, causing an increase in the magnitude of Z_C and a drop in its phase. Unfortunately the lumped element model of the round window is not very accurate in this frequency region, as seen in Appendix A, since both the stapes motion (Sim et al., 2010) and the round window motion (Kwacz et al., 2011) become more complicated than the in-phase behaviour seen at low frequencies.

When the round window stiffness is increased by a factor of 10, Z_C is dominated by the inertance of the VA at low frequencies, but this then combines with the compliance of the RW to give a parallel resonance at about 200 Hz and hence a peak in the cochlear impedance, as can be verified by noting the crossover point for these two impedances in Fig. 7. As the round window stiffness is further increased, the frequency range over which Z_C is dominated by L_{VA} increases and the resonance is pushed up to about 800 Hz and 2.5 kHz when C_{RW} is 1/100 or 1/1000 of its nominal value. The dominant acoustic resistance in the circuit for Z_C is R_{WA}, and so the Q of this resonance, Q_C, is approximately given by

$$Q_C = \frac{1}{R_{WA}}\sqrt{\frac{L_{VA}}{C_{RW}}}, \tag{5}$$

so that Q_C increases as C_{RW} decreases, as seen in Fig. 8.

The predicted change in the input impedance at the tympanic membrane can also be calculated using a two-port model for the

Fig. 7. The variation in the impedances of the various components in Fig. 6 over the frequency range of interest. Since a log-log scale is used, the impedances of the inertances rise at 1 decade/decade and those of the compliances fall at 1 decade/decade. This graph will be used to help understand the results presented in Sections 5 and 6.
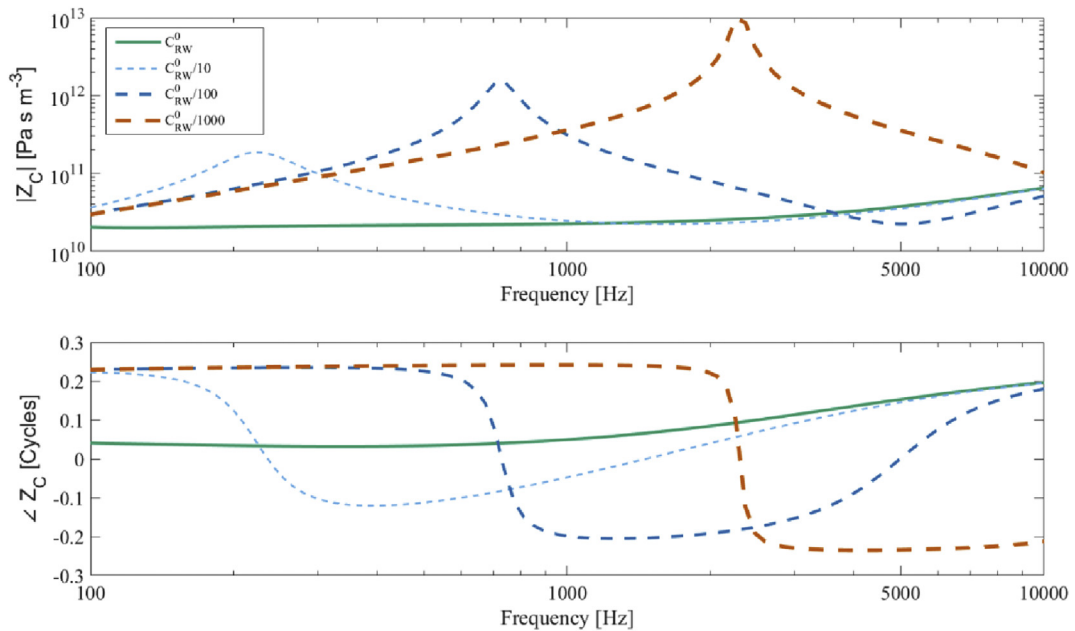
Fig. 8. The calculated magnitude and phase of the cochlear input impedance, Z_C, when the stiffness of the round window takes its normal value and when it is increased by a factor of 10, 100, or 1000.

middle ear, Peake et al. (1992), Shera and Zweig (1992) and Puria (2003). In such a model the acoustic pressure in the ear canal next to the tympanic membrane, at the ear drum, p_{ed}, and the acoustic volume velocity of the tympanic membrane, q_{ed}, are related to the pressure in the scala vestibuli next to the stapes, p_{st}, and the volume velocity of the stapes, q_{st}, by the equations

$$p_{ed} = Ap_{st} + Bq_{st}, \tag{6}$$

$$q_{ed} = Cp_{st} + Dq_{st}, \tag{7}$$

where both volume velocities are define looking into the ear, p_{st} here is equal to p_{SV} in Fig. 6, and A, B, C and D are complex, frequency-dependent parameters.

Since the ratio of p_{st} to q_{st} is equal to the cochlear input impedance Z_C, the acoustic input impedance at the tympanic membrane is readily calculated as

$$\frac{p_{ed}}{q_{ed}} = \frac{AZ_C + B}{CZ_C + D}. \tag{8}$$

The parameters A, B, C and D in the two-port equations have been calculated using the model of Kringlebotn (1988), as

implemented Ku (2008), and hence the acoustic impedance at the tympanic membrane has been calculated using equation (8). Fig. 9 shows the magnitude and phase of the predicted tympanic membrane impedance, calculated with the cochlear input impedances shown in Fig. 8 for the normal round window stiffness and when this is increased by factors of 10, 100 and 1000. Also shown in this figure is the predicted impedance at the tympanic membrane when the stapes are completely blocked, so that the Z_C tends to an infinite value. The predicted tympanic membranes under normal and this blocked condition are similar to those measured for example by Zwislocki (1962), Shaw and Stinson (1981), as quoted in Kringlebotn, (1988) and Voss et al. (2000), which provide some confidence in the middle ear model. In contrast to the relatively smooth variation in the tympanic membrane impedance under

the frequency response of the tympanic membrane impedance might provide a relatively simple clinical test for the presence of round window stiffening. The frequency of this peak may vary significantly with the size or the patency of the vestibular aqueduct in a particular patient, however, and clearly further work is required to validate this prediction.

6. Prediction of the hearing loss

The lumped element circuit in Fig. 5 can be used to calculate the pressure across the BM, p_{BM}, which generates the slow wave that eventually excites the inner hair cells in the cochlea, as a function of the blocked middle pressure, p_{ME}, as

$$\frac{p_{BM}}{p_{ME}} = \frac{Z_{BM}Z_{VA}(Z_{RW} + Z_{CA})}{Z_{BM}(Z_{VA} + Z_{ME})(Z_{RW} + Z_{CA}) + Z_{CA}Z_{RW}(Z_{VA} + Z_{ME}) + Z_{VA}Z_{ME}(Z_{RW} + Z_{CA})}. \tag{9}$$

these two conditions, at frequencies below about 1 kHz, this impedance shows a more complicated behaviour if the round window stiffness is increased. A dip at about 250 Hz and then a peak at about 320 Hz is observed, for example, when the round window stiffness is increased by a factor of 100. The dynamics of the middle ear are largely governed by its stiffness below about 1 kHz and the peak in the impedance described above appears to be the result of a series resonance between the compliance of the middle ear and the inertance of the vestibular aqueduct, since the latter dominates Z_C at low frequencies, as seen in Fig. 8. This suggestion is supported by other simulations, not shown here, where the vestibular aqueduct inertance was doubled in the equivalent circuit for Z_C, in which case the frequency of the peak in the tympanic membrane impedance dropped by a factor of about the square root of 2.

These results suggest that the presence of this dip and peak in

The Thévenin equivalent pressure and impedance in Fig. 5 provide a complete model of the linear behaviour of the middle ear in this impedance model, provided that the pressure in the middle ear, which is affected by the volume velocity of the round window, only plays a minor role in middle ear transmission compared with the direct mechanical path (Shera and Zweig, 1992), as does appear to be a reasonable assumption in the frequency range of interest here (Keefe, 2015). The changes in the ratio of p_{BM} to p_{ME} as the RW is stiffened can be taken as a measure of the change of the acoustic excitation of the cochlea.

Fig. 10 shows the calculated variation of the magnitude and phase of p_{BM}/p_{ME} with frequency as the round window stiffness is increased. Under normal circumstances Z_{RW} is small compared to Z_{BM}, which is itself small compared to Z_{VA} and Z_{CA}, so that the ratio of these pressures is given approximately by
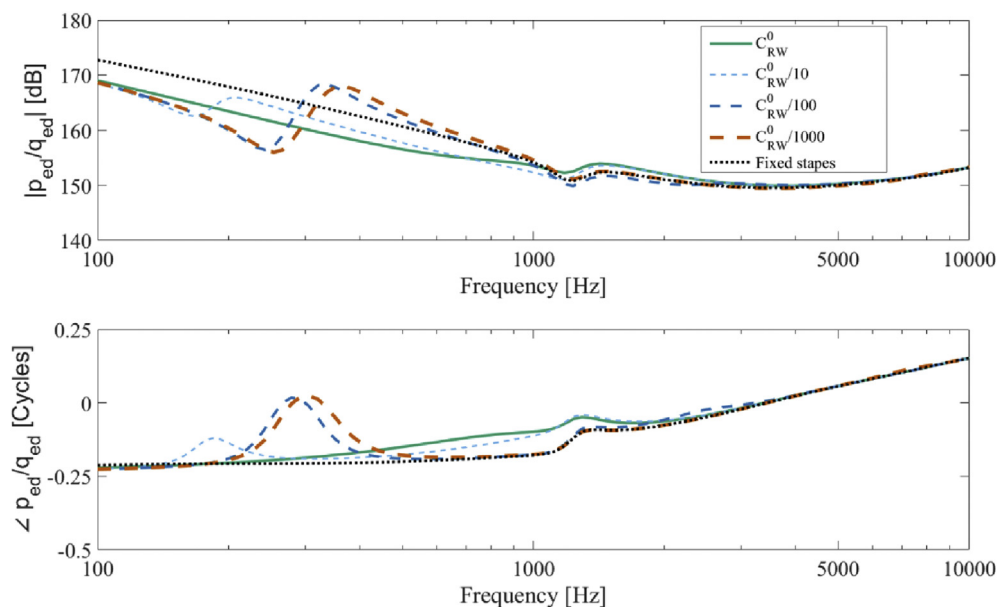

Fig. 9. The calculated magnitude and phase of the acoustic impedance at the tympanic membrane, calculated using Kringlebotn's (1988) two-port network model for the middle ear, and the cochlear input impedance shown in Fig. 8, when the round window stiffness takes its normal value, when it is increased by a factor of 10, 100 or 1,000, and also when the stapes are assumed to be fixed.
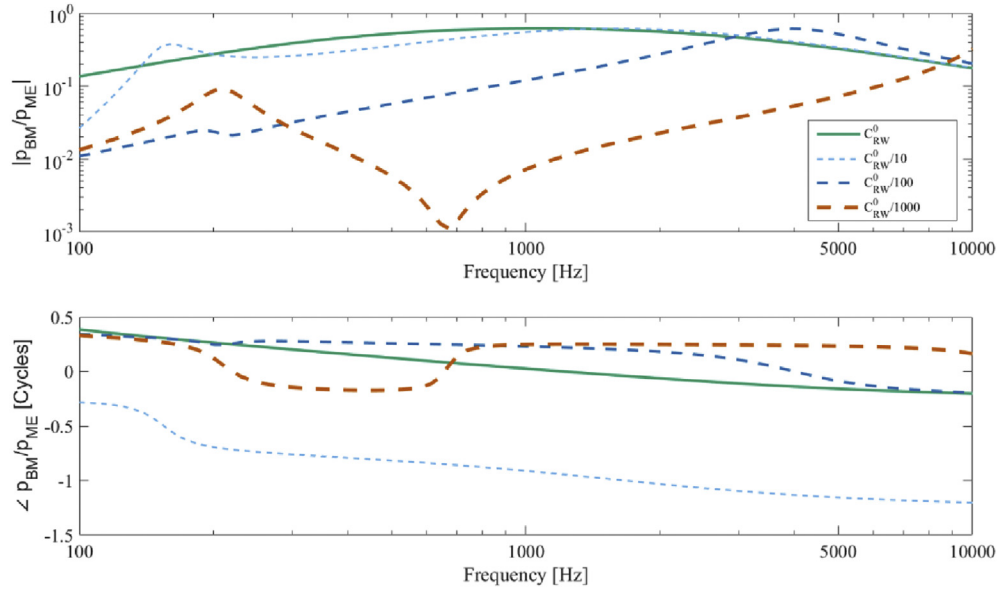
Fig. 10. The variation of the magnitude and phase of p_{BM}/p_{ME} with frequency when the stiffness of the round window takes its normal value and when it is increased by a factor of 10, 100, or 1000.

$$\left.\frac{p_{BM}}{p_{ME}}\right|_{C_{RW}^0} \approx \frac{Z_{BM}}{Z_{BM} + Z_{ME}}. \tag{10}$$

This equation predicts the results in Fig. 10 under normal conditions reasonably well, with the ratio of pressures showing a broad peak at the series resonance frequency of L_{ME} and C_{ME}, which is seen to occur at about 1.5 kHz in Fig. 7.

If the round window stiffness is increased by a factor of 10, the compliances that dominate the response at low frequencies become C_{RW} and C_{ME}, and a well damped peak is generated when the combined compliance resonates with L_{VA} at about 150 Hz, but the higher frequency response is largely unchanged.

When the round window stiffness is increased by a factor of 100, the compliance that dominates at low frequencies is then C_{ME}, so that the response is reduced, and this compliance then resonates with L_{VA} to give a well-damped peak in the response at about 200 Hz. Above 200 Hz the dynamics are dominated by C_{RW} and R_{WA}, so that the response increases with frequency, until C_{RW} has a well-damped resonance with L_{RW} at about 5 kHz, as can again be deduced from Fig. 7.

When the stiffness is increased by a factor of 1,000, then a parallel resonance occurs between C_{RW} and L_{CA} at about 700 Hz, generating a high impedance in the parallel combination of Z_{RW} and Z_{CA}, below Z_{BM} in Fig. 7, and reducing the volume velocity supplied by p_{ME} to generate a notch in the response. Above this frequency the dynamics are again dominated by C_{RW} and R_{WA}, although C_{RW} is now reduced compared with the cases considered above, and so too is the response.

The predicted hearing loss due to the stiffening of the round window is shown in Fig. 11, over the frequency range shown for the measured results in Fig. 1, as calculated by the level of p_{BM} under normal conditions divided by p_{BM} under the stiffened condition. This quantity is equal to 0 dB, by definition, under normal conditions, but is also not greatly affected if the RW stiffness is increased by a factor of 10. As the stiffness increases by a factor of 100, however, the hearing loss is predicted to be about 22 dB at 250 Hz, gradually falling to about 15 dB at 1 kHz. When the stiffness is increased by a factor of 1,000, the predicted hearing loss gets

considerably greater at about 700 Hz due to the parallel resonance between C_{RW} and L_{CA}

So, if the RW stiffness is assumed to be increased by about a factor of 100, as predicted for cochlear implant insertion in the finite element model, the lumped element model predicts approximately the same average level of residual hearing loss below 1 kHz as is shown in Fig. 1, and also as reported for other clinical data by Adunka et al. (2013) and Friedmann et al. (2015).

7. Variability in the hearing loss

The results in Fig. 11 indicate the change in the predicted hearing loss with RW stiffness, for a given size of cochlear and vestibular aqueducts, as discussed in Section 4.4. There is, in fact, considerable variability in the sizes and patencies of these aqueducts from person to person, as discussed above. The normal variation in the length of the cochlear aqueduct seems to be from about 6 mm to about 12 mm and the normal variation in the diameter is from about 0.02 mm to 0.15 mm (Gopen et al., 1997). There may be even larger variations in the size of the vestibular aqueduct, where there has been some debate about what constitutes an abnormally large aqueduct in large vestibular aqueduct syndrome. The normal variation in its diameter at the axial midpoint appears to be from about 0.4 mm to 0.9 mm and in its diameter at the coronal midpoint from about 0.5 mm to 1.9 mm (Saliba et al., 2012), although it is actually the diameter at the narrowest point that has the greatest effect on the impedance. By re-calculating the inertances for different sizes of the aqueducts, an ensemble of predictions for the hearing loss can be calculated. The RW compliance has also been assumed to vary over a range of values from $C_{RW} = C_{RW}^0/50$, to represent the effect of a smaller CI, to $C_{RW} = C_{RW}^0/200$, to represent the effect of a larger CI, both with some thickening of the round window.

Fig. 12 shows the results of these simulations and, for clarity, only the upper and lower boundaries of this set of calculated hearing losses are shown, together with the average value over all these simulations, although this average clearly does not account for the true distribution of these geometric parameters, since these are not known. In general with a stiffened round window, an
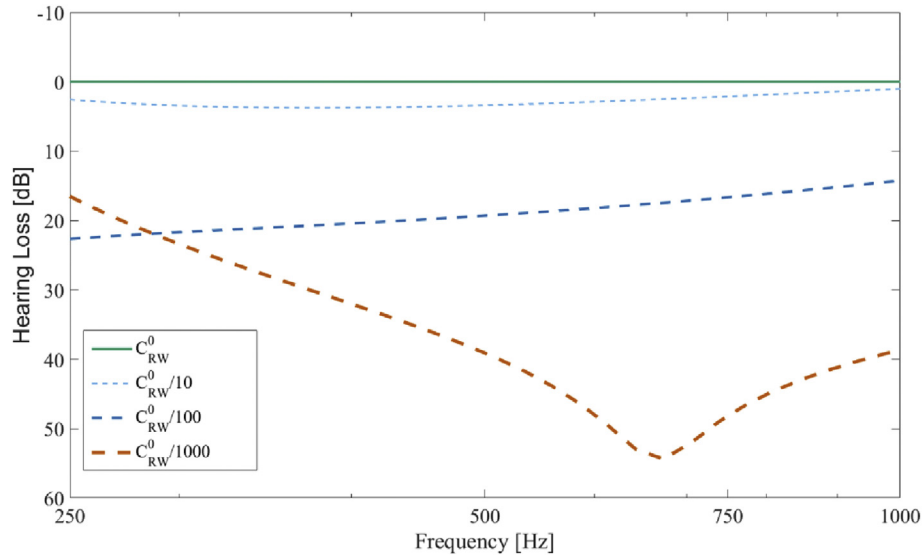
Fig. 11. The predicted loss of residual hearing due to the stiffening of the round window, plotted over the same frequency range as in Fig. 1.
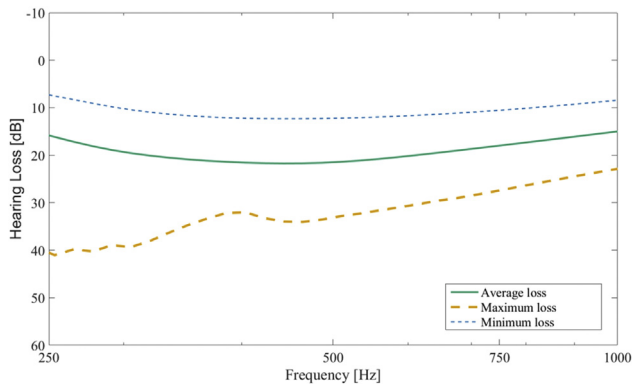

Fig. 12. Predicted hearing loss using the lumped element model when the length and diameter of VA and CA are assumed to vary over the range discussed in the text, and the round window stiffness is assumed to be either 50, 100 or 200 times greater than its normal condition. Green line for average result, blue dashed line for lower boundary of hearing loss, and orange dashed line for upper boundary of hearing loss. (For interpretation of the references to colour in this figure legend, the reader is referred to the web version of this article.)

enlarged VA gives a greater predicted hearing loss, whereas an enlarged CA reduces the predicted hearing loss, at least at the lower frequencies.

The resulting variation in the predicted hearing loss from the average value is about +25 to −8 dB at 250 Hz, falling to about ±8 dB at 1 kHz. This predicted variation may go some way towards explaining the large individual variations in the measurements of the additional hearing loss after cochlear implantation, as discussed in the introduction.

8. Reduction of hearing loss with an artificial compliant element

If a significant component of the loss in residual hearing after cochlear implantation is due to a stiffening, or loss of compliance, of the round window, it may be possible to recover some of this residual hearing by introducing an artificially compliant element, perhaps into the cochlear implant itself.

For example a small bubble of gas might be introduced into the cochlear implant such that it is positioned in the scala tympani, close to the round window, and coupled to the fluid via a flexible window. The acoustic compliance of such a gas bubble is given by

$$C_B = \frac{V_B}{\gamma P_B}, \tag{11}$$

where V_B is the volume of the bubble, γ is the ratio of principal specific heats for the gas and P_B is the pressure in the gas bubble. The adiabatic bulk modulus of the gas, which is given by γP_B, is about 1.4×10^5 Pa for air at atmosphere pressure, and this is very much less than the corresponding value for the bulk modulus of the cochlear fluid, which can be calculated from ρc^2 as about 2×10^9 Pa. Only a very small gas bubble is thus required to give a significant change in the compliance. A 0.15 mm³ bubble of air at atmosphere pressure, for example, has an acoustic compliance of about 1×10^{-13} N^{-1} m⁵, which is the same as that of the intact round window. The compliance of the gas bubble would, however, be affected by the flexible window connecting it to the fluid. Ravicz et al. (2015) have described a similar compliant element, but for the treatment of fluid in the middle ear, and the balloon used to enclose the air bubble in this case approximately halved the compliance of the bubble, in the worst case. Thus doubling the size of the bubble, to 0.3 mm³ would still provide the required compliance, even when enclosed in such a balloon, and would still be small in comparison with the 30 mm³ or so volume of the scala tympani (Thorne et al., 1999).

Fig. 6 also includes the acoustic compliance of such a gas bubble, C_B, near the round window. The compliance of the bubble effectively appears in parallel with the inertance of the cochlear aqueduct. Assuming a 0.15 mm³ bubble of air at atmosphere pressure, with a compliance as calculated above, the hearing loss with the air bubble has been calculated, for the same range of RW stiffness as shown in Fig. 11. The loss of residual hearing with the bubble is predicted to be less than 1 dB for all these values of round window stiffness.

9. Discussion and conclusions

It has been found in several centres that the loss of low-frequency residual hearing after cochlear implantation is about

20 dB. This loss may be due to many factors, which include the stiffening of the round window due to the presence of the cochlea implant. A finite element model has been used to investigate this stiffening effect, and it is shown that the stiffness of the round window is increased by about a factor of 100 by the presence of the cochlear implant for frequencies below 1 kHz. The dynamics of the cochlea implant and the round window are likely to be more complicated than this, particularly at higher frequencies, however, since the cochlea implant probably does move to some extent (Semmelbauer and Böhnke, 2016), and also because the round window is probably also thickened as it heals around the cochlear implant. Nevertheless this simple model appears to give a reasonable first approximation to the change in its dynamics.

A lumped element model is then used to calculate the effect of this stiffening of the round window on the excitation of the cochlea. The parameters for this model are taken from measurements in the literature and it is found to be important to include the effects of the cochlea and vestibular aqueducts, since their presence become more important as the round window stiffness is increased.

For a 100-fold increase in the round window stiffness, as predicted by the finite element model, the loss of residual hearing is predicted to be about 22 dB at 250 Hz, falling to about 15 dB at 1 kHz, in reasonably good agreement with the average hearing loss after implantation measured at several centres. It thus appears that this stiffening is a significant cause of the hearing loss generally observed after cochlea implant surgery.

By assuming reasonable variations in the dimensions of the aqueducts and in the stiffness of the round window, significant variability in the predicted loss of residual hearing is observed, which is also in good agreement with the clinical measurements.

It may be possible to recover some of the residual hearing lost by the stiffening of the round window by artificially introducing a compliant element near the round window. The effect of a $0.15~\text{mm}^3$; bubble of air has been considered, for example, when incorporated into the cochlea implant and positioned inside the scala tympani close to the round window, and coupled to the fluid via a flexible window. This significantly reduces the predicted loss of residual hearing.

Appendix A. The effect of stapes rocking on the estimation of round window impedance

Nakajima et al. (2009) estimated the round window impedance from measurements of pressure in the scala tympani near the round window, p_{ST}, and estimates of the stapes volume velocity, $\widehat{q}_{st}$, as

$$\widehat{Z}_{RW} = \frac{p_{ST}}{\widehat{q}_{st}}, \tag{A1}$$

where $\widehat{q}_{st} = A_{st} \widehat{V}_{st}$, A_{st} and $\widehat{V}_{st}$ are the area and estimated linear velocity of the stapes, and also assuming.

1) The volume velocity of oval window is equal to that of the round window
2) The stapes motion is piston-like

Similar measurements and assumptions are made by Aibara et al. (2001) and Puria (2003). Actually $\widehat{V}_{st}$ is measured at the posterior crus and the stapes are known to rock at higher frequencies, e.g. Sim et al. (2010), so that

$$\widehat{V}_{st} = V_{st} + V_{rock}, \tag{A2}$$

where V_{st} is the component of velocity due to the piston-like motion and V_{rock} is that due to the rocking motion. Equation (A1) thus takes the form

$$\widehat{Z}_{RW} = \frac{p_{ST}}{A_{st}(V_{st} + V_{rock})}, \tag{A3}$$

whereas the true value of the round window impedance is given by

$$Z_{RW} = \frac{p_{ST}}{A_{st} V_{st}} = \widehat{Z}_{RW}\left(1 + \frac{V_{rock}}{V_{st}}\right), \tag{A4}$$

The ration V_{rock}/V_{st} is given by Hato et al. (2003) and Fig. 8 C and D in Sim et al. (2010). Using the Hato et al. (2003) results, we can estimate that.

at 0.5 kHz $V_{rock}/V_{st} \approx 0.1$ with little phase shift,
at 5 kHz $V_{rock}/V_{st} \approx 1$ with a phase shift about 45°, and
at 8 kHz $V_{rock}/V_{st} \approx 1.6$ with phase shift of greater than 90°.

So, empirically fitting this data with

$$\left|\frac{V_{rock}}{V_{st}}\right| \approx \frac{f}{5000}, \quad \angle\frac{V_{rock}}{V_{st}} \approx 0.78\frac{f}{5000}, \tag{A5}$$

where f is frequency in Hz and the phase is in radians, the corrected mean value of the round window impedance is given by

$$Z_{RW} = \frac{p_{ST}}{V_{st}} = \widehat{Z}_{RW}\left[1 + \left(\frac{f}{5000}\right)e^{i(0.78f/5000)}\right]. \tag{A6}$$

Fig. A1 shows the original mean values of the estimated round window impedance, $\widehat{Z}_{RW}$, from Nakajima et al. (2009) and the value of this impedance corrected for the stapes rocking, Z_{RW}, as above. Also shown is a fitted mass-spring-damper model, which fits the modulus of the corrected model reasonably well up to about 5 kHz, although the predicted phase is somewhat larger than that measured, even after correction. It is known, however, that the motion of both the stapes and of the round window becomes more complicated above 5 kHz (Stenfelt et al., 2004; Kwacz et al., 2011) and the effect of multiple, well damped, structural modes may well account for the observed high-frequency behaviour, as suggested by the results of the simple finite element model in Section 2. The low-frequency model of the round window impedance used here thus takes the form shown in equation (A8).

$$Z_{RW} = i\omega L_{RW} + R_{RW} + \frac{1}{i\omega C_{RW}}, \tag{A7}$$

with the fitted parameters $C_{RW} = 1 \times 10^{-13}~\text{m}^5\text{N}^{-1}$, $L_{RW} = 1 \times 10^6~\text{N s}^2\text{m}^{-5}$ and $R_{RW} = 2.5 \times 10^9~\text{N s m}^{-5}$, as used in Table 1.
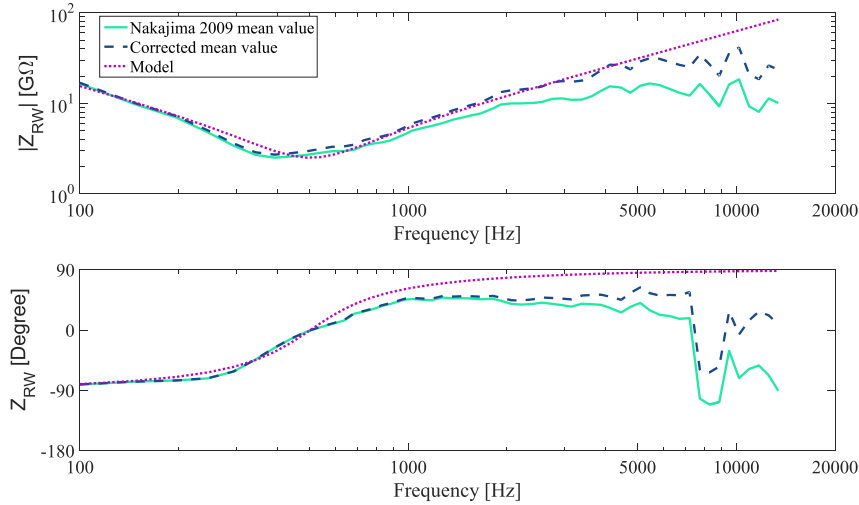
Fig. A1. The impedance of round window.

Appendix B. Acoustic impedance of the cochlear aqueduct and vestibular aqueduct

The acoustic properties of the two aqueducts is modelled by Stenfelt (2015) as being that of a fluid-filled cylindrical duct that terminates in a larger fluid-filled space, corresponding to the cranial cavity, and the acoustic impedance thus takes the form

$$Z_A = i\omega L_D + R_D - i/\omega C_C,$$ (B1)

where L_D and R_D are the acoustic inertance and resistance of the duct and C_C is the acoustic compliance of the cavity. This compliance can be written as

$$C_C = \frac{V}{\rho c^2},$$ (B2)

where ρ and c are the density and speed of sound of the fluid and V is volume of the cranial space. Although it may initially be though that the fluid-filled cavity would provide a very high impedance to terminate the duct, this turns out not to be the case, since its impedance is small in comparison with the inertance of the duct in the frequency range of interest here, i.e. above 100 Hz. In Stenfelt (2015), and the earlier work of Gopen et al. (1997), the inertance and resistance of the duct are also calculated as if their radius is small compared with the viscous boundary layer thickness, i.e. a "tube of very small radius" in the terms of Beranek (1954). The viscous boundary layer thickness is given by

$$\delta = \sqrt{\frac{\eta}{\rho\omega}},$$ (B3)

where η is the coefficient of viscosity, which is about 7×10^{-4} kg m^{-1} s^{-1} for cochlear fluids at body temperature. At 100 Hz, this boundary layer thickness is thus about 30 μm for cochlear fluids, so that the radius of the cochlear aqueduct, 75 μm, and the smallest radius of the vestibular aqueduct, 150 μm, assumed by Stenfelt (2015), are actually not small compared with the viscous boundary layer thickness.

It is thus more appropriate to use the inertance and resistance of an "intermediate size tube", in the terms used by Beranek (1954), which in, our notation, are

$$L_D = \frac{\rho l}{\pi a^2},$$ (B4)

$$R_D = \frac{l}{\pi a^3}\sqrt{\frac{\eta\omega\rho}{2}},$$ (B5)

where a is the duct radius and it should be noted that Beranek uses the kinematic coefficient of viscosity, η/ω, and that he has an additional factor of two to account for thermal losses in air, which do not apply to the fluid case here since the Prandtl number is large (Baumgart, 2010). The dimensions of the aqueducts are taken from Stenfelt (2015); to be of length 10 mm and diameter 0.15 mm for the cochlear aqueduct and for the vestibular aqueduct to be the combination of a duct of length 1.5 mm with a diameter of 0.3 mm and a duct of length 8.5 mm with a diameter of 0.6 mm, and the cranial space is assumed to be a sphere of radius 50 mm, and the various terms in equation (B1) can be calculated, using equations (B2), (B4) and (B5).

Fig. B1 shows the magnitude of this impedance for the two aqueducts, calculated from equation (B1), over a broader frequency range than that used above to show the overall behaviour.
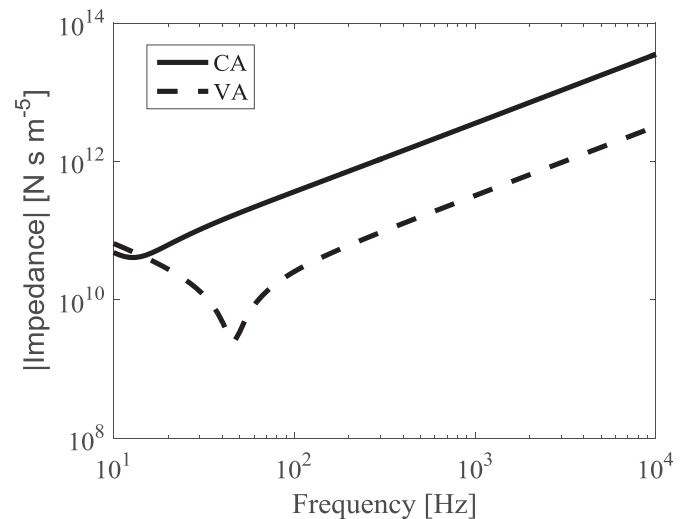

Fig. B1. The magnitude of the acoustic impedance for the cochlear aqueduct, CA, and vestibular aqueduct, VA, calculated using equations (B1), (B2), (B4) and (B5).

It can be seen that the series resonance of L_D and C_C occurs below 100 Hz in both cases, and that above this frequency, the two impedances are well approximated by the corresponding inertances and resistances, as used in the main text above. Strictly speaking the equations used for L_D and R_D in this calculation are somewhat inaccurate at the lowest frequency shown in Fig. B1, 10 Hz, since the viscous boundary layer thickness is then no longer small compared with the duct radius, but the conclusions for the approximations above 100 Hz still hold.

The difference between these inertances and those used by Stenfelt (2015) is only a factor of 4/3, however, and, over the frequency range of his results, the duct resistance plays a relatively minor role, so that the conclusions of this paper are not significantly affected by these modifications to the form of the duct impedances.

References

Adunka, O.F., Dillon, M.T., Adunka, M.C., King, E.R., Pillsbury, H.C., Buchman, C.A., 2013. Hearing preservation and speech perception outcomes with electric-acoustic stimulation after 12 months of listening experience. Laryngoscope 123, 2509–2515.

Aibara, R., Welsh, J.T., Puria, S., Goode, R.L., 2001. Human middle-ear sound transfer function and cochlear input impedance. Hear Res. 152, 100–109.

Atturo, F., Barbara, M., Rask-Andersen, H., 2014. Is the human round window really round? an anatomic study with surgical implications. Otol. Neurotol. 35, 1354–1360.

Baumgart, J., 2010. The Hair Bundle: Fluid-structure Interaction in the Inner Ear. PhD Thesis. der Technischen Universitat Dresden, Dresden.

Beranek, L.L., 1954. Acoustics. American Institute of Physics, New York.

Cai, Q., Whitcomb, C., Eggleston, J., Sun, W., Salvi, R., Hu, B.H., 2013. Round window closure affects cochlear responses to suprathreshold stimuli. Laryngoscope 123, E116–E121.

Causon, A., Verschuur, C., Newman, T.A., 2015. A retrospective analysis of the contribution of reported factors in cochlear implantation on hearing preservation outcomes. Otol. Neurotol. 36, 1137–1145.

Choi, C.-H., Oghalai, J.S., 2005. Predicting the effect of post-implant cochlear fibrosis on residual hearing. Hear Res. 205, 193–200.

Dallos, P., 1970. Low-frequency auditory characteristics: species dependence. J. Acoust. Soc. Am. 48, 489–499.

Franke, R., Dancer, A., Buck, K., Evrard, G., Lenoir, M., 1985. Hydromechanical cochlear phenomena at low frequencies in Guinea pig. Acustica 59, 30–41.

Friedmann, D.R., Peng, R., Fang, Y., McMenomey, S.O., Roland, J.T., Waltzman, S.B., 2015. Effects of loss of residual hearing on speech performance with the CI422 and the Hybrid-L electrode. Cochlear implants Int. 16, 277–284.

Gifford, R.H., Dorman, M.F., Skarzynski, H., Lorens, A., Polak, M., Driscoll, C.L., Roland, P., Buchman, C.A., 2013. Cochlear implantation with hearing preservation yields significant benefit for speech recognition in complex listening environments. Ear Hear 34, 413–425.

Gopen, Q., Rosowski, J.J., Merchant, S.N., 1997. Anatomy of the normal human cochlear aqueduct with functional implications. Hear Res. 107, 9–22.

Grant, H., 1973. Round window occlusion in otosclerosis. J. Laryngol. Otol. 87, 21–26.

Hato, N., Stenfelt, S., Goode, R.L., 2003. Three-dimensional stapes footplate motion in human temporal bones. Audiol. Neurootol 8, 140–152.

Helbig, S., Van de Heyning, P., Kiefer, J., Baumann, U., Kleine-Punte, A., Brockmeier, H., Anderson, I., Gstoettner, W., 2011. Combined electric acoustic stimulation with the PULSARCI(100) implant system using the FLEX(EAS) electrode array. Acta Otolaryngol. 131, 585–595.

Keefe, D.H., 2015. Human middle-ear model with compound eardrum and airway branching in mastoid air cells. J. Acoust. Soc. Am. 137, 2698–2725.

Kringlebotn, M., 1988. Network model for the human middle ear. Scand. Audiol. 17, 75–85.

Ku, E.M., 2008. Modelling the Human Cochlea. PhD Thesis. University of Southampton, Southampton. http://eprints.soton.ac.uk/64535/.

Kwacz, M., Mrowka, M., Wysocki, J., 2011. Round window membrane motion before and after stapedotomy surgery - an experimental study. Acta Bioeng. Biomech. 13, 27–33.

Kwacz, M., Marek, P., Borkowski, P., Mrowka, M., 2013. A three-dimensional finite element model of round window membrane vibration before and after stapedotomy surgery. Biomech. Model Mechanobiol. 12, 1243–1261.

Li, P.M., Wang, H., Northrop, C., Merchant, S.N., Nadol Jr., J.B., 2007. Anatomy of the round window and hook region of the cochlea with implications for cochlear implantation and other endocochlear surgical procedures. Otol. Neurotol. 28, 641–648.

Lynch, T.J., Nedzelnitsky, V., Peake, W.T., 1982. Input impedance of the cochlea in cat. J. Acoust. Soc. Am. 72, 108–130.

Marquardt, T., Hensel, J., 2013. A simple electrical lumped-element model simulates intra-cochlear sound pressures and cochlear impedance below 2 kHz. J. Acoust. Soc. Am. 134, 3730–3738.

Nageris, B.I., Attias, J., Shemesh, R., Hod, R., Preis, M., 2012. Effect of cochlear window fixation on air- and bone-conduction thresholds. Otol. Neurotol. 33, 1679–1684.

Nakajima, H.H., Dong, W., Olson, E.S., Merchant, S.N., Ravicz, M.E., Rosowski, J.J., 2009. Differential intracochlear sound pressure measurements in normal human temporal bones. JARO 10, 23–36.

Nikkar-Esfahani, A., Whelan, D., Banerjee, A., 2013. Occlusion of the round window: a novel way to treat hyperacusis symptoms in superior semicircular canal dehiscence syndrome. J. Laryngol. Otol. 127, 705–707.

Peake, W.T., Rosowski, J.J., Lynch 3rd, T.J., 1992. Middle-ear transmission: acoustic versus ossicular coupling in cat and human. Hear Res. 57, 245–268.

Pfingst, B.E., Zhou, N., Colesa, D.J., Watts, M.M., Strahl, S.B., Garadat, S.N., Schwartz-Leyzac, K.C., Budenz, C.L., Raphael, Y., Zwolan, T.A., 2015. Importance of cochlear health for implant function. Hear Res. 322, 77–88.

Puria, S., 2003. Measurements of human middle ear forward and reverse acoustics: implications for otoacoustic emissions. J. Acoust. Soc. Am. 113, 2773–2789.

Puria, S., Allen, J.B., 1991. A parametric study of cochlear input impedance. J. Acoust. Soc. Am. 89, 287–309.

Quesnel, A.M., Nakajima, H.H., Rosowski, J.J., Hansen, M.R., Gantz, B.J., Nadol Jr., J.B., 2016. Delayed loss of hearing after hearing preservation cochlear implantation: human temporal bone pathology and implications for etiology. Hear Res. 333, 225–234.

Ravicz, M.E., Chien, W.W., Rosowski, J.J., 2015. Restoration of middle-ear input in fluid-filled middle ears by controlled introduction of air or a novel air-filled implant. Hear Res. 328, 8–23.

Richard, C., Fayad, J.N., Doherty, J., Linthicum Jr., F.H., 2012. Round window versus cochleostomy technique in cochlear implantation: histologic findings. Otol. Neurotol. 33, 1181–1187.

Rubel, E.W., Furrer, S.A., Stone, J.S., 2013. A brief history of hair cell regeneration research and speculations on the future. Hear Res. 297, 42–51.

Saliba, I., Gingras-Charland, M.E., St-Cyr, K., Decarie, J.C., 2012. Coronal CT scan measurements and hearing evolution in enlarged vestibular aqueduct syndrome. Int. J. Pediatr. Otorhinolaryngol. 76, 492–499.

Santa Maria, P.L., Gluth, M.B., Yuan, Y., Atlas, M.D., Blevins, N.H., 2014. Hearing preservation surgery for cochlear implantation: a meta-analysis. Otol. Neurotol. 35, e256–269.

Semmelbauer, S., Böhnke, F., 2016. Influence of the Cochlear Implant Electrode on the Traveling Wave Propagation. Klinikum rechts der Isar der TUM (Internal report).

Seyyedi, M., Nadol Jr., J.B., 2014. Intracochlear inflammatory response to cochlear implant electrodes in humans. Otol. Neurotol. 35, 1545–1551.

Shaw, E.A.G., Stinson, M.R., 1981. Network concepts and energy flow in the human middle-ear. J. Acoust. Soc. Am. 69, S43.

Shera, C.A., Zweig, G., 1992. Middle-ear phenomenology: the view from the three windows. J. Acoust. Soc. Am. 92, 1356–1370.

Silverstein, H., Kartush, J.M., Parnes, L.S., Poe, D.S., Babu, S.C., Levenson, M.J., Wazen, J., Ridley, R.W., 2014. Round window reinforcement for superior semicircular canal dehiscence: a retrospective multi-center case series. Am. J. Otolaryngol. 35, 286–293.

Sim, J.H., Chatzimichalis, M., Lauxmann, M., Roosli, C., Eiber, A., Huber, A.M., 2010. Complex stapes motions in human ears. JARO 11, 329–341.

Stenfelt, S., 2015. Inner ear contribution to bone conduction hearing in the human. Hear Res. 329, 41–51.

Stenfelt, S., Hato, N., Goode, R.L., 2004. Round window membrane motion with air conduction and bone conduction stimulation. Hear Res. 198, 10–24.

Talbot, K.N., Hartley, D.E., 2008. Combined electro-acoustic stimulation: a beneficial union? Clin. Otolaryngol. 33, 536–545.

Thorne, M., Salt, A.N., DeMott, J.E., Henson, M.M., Henson Jr., O.W., Gewalt, S.L., 1999. Cochlear fluid space dimensions for six species derived from reconstructions of three-dimensional magnetic resonance images. Laryngoscope 109, 1661–1668.

Toth, M., Alpar, A., Patonay, L., Olah, I., 2006. Development and surgical anatomy of the round window niche. Ann. Anat. 188, 93–101.

Van Valkenburg, M.E., 1974. Network Analysis 3rd Edition. Prentice Hall, New Jersey.

Verschuur, C., Hellier, W., Teo, C., 2016. An evaluation of hearing preservation outcomes in routine cochlear implant care: implications for candidacy. Cochlear implants Int. 17, 62–65.

Verschuur, C., Boland, C., Frost, E., Constable, J., 2013. The role of first formant information in simulated electro-acoustic hearing. J. Acoust. Soc. Am. 133, 4279–4289.

Voss, S.E., Rosowski, J.J., Merchant, S.N., Peake, W.T., 2000. Acoustic responses of the human middle ear. Hear Res. 150, 43–69.

Zhang, T., Dorman, M.F., Spahr, A.J., 2010. Information from the voice fundamental frequency (F0) region accounts for the majority of the benefit when acoustic stimulation is added to electric stimulation. Ear Hear 31, 63–69.

Zhang, X., Gan, R.Z., 2013. Dynamic properties of human round window membrane in auditory frequencies running head: dynamic properties of round window membrane. Med. Eng. Phys. 35, 310–318.

Zwislocki, J., 1962. Analysis of the middle-ear function. Part I: input impedance. J. Acoust. Soc. Am. 34, 1514–1523.